CMS Physics Analysis Summary

Contact: cms-pog-conveners-lum@cern.ch 2016/03/12

CMS Luminosity Measurement for the 2015 Data Taking Period

The CMS Collaboration

Abstract

The measurement of the integrated luminosity delivered to the CMS Experiment during the 2015 LHC proton-proton run at 13 TeV center-of-mass energy is presented. The Pixel Cluster Counting method is used and the absolute luminosity scale calibration is derived from an analysis of Van der Meer Scans performed in August 2015. The overall uncertainty on the luminosity measurement is estimated to be 2.7%.

1 Introduction

After the completion of the Run 1 LHC program providing proton-proton collisions at a center-of-mass energy of 7 and 8 TeV and 50 ns bunch spacing, a re-calibration of the CMS sub-detectors used for luminosity measurements to the LHC Run 2 conditions characterized by 25 ns bunch spacing and proton-proton collisions at $\sqrt{s} = 13$ TeV is necessary.

CMS uses five detectors to monitor and measure luminosity based on rate measurements of a variety of observables: the CMS silicon pixel detector, the Drift Tubes in the barrel (DT), the Forward Hadronic Calorimeter (HF), the Fast Beam Condtions Monitore (BCM1f) and the newly installed and commissioned Pixel Luminosity Telescope (PLT). The PLT, BCM1f and HF monitor luminosity via a fast readout system which is asynchronous with the readout of the CMS experimental apparatus. The silicon pixel detector and DT are featured by very low occupancy and good stability over time. These two detectors utlize the standard CMS trigger and data aquisition systems.

Absolute calibrations of the detectors according to the specific rate algorithms are established by conducting Van der Meer (VdM) scans performed with a dedicated LHC machine set up. By scanning the two beams through one another in the transverse plane of the detector VdM scans allow to measure the luminosity per colliding bunch pair from machine parameters [1]. This method has already previously been used by the LHC experiments during Run 1 [2–5] enabling the CMS Experiment to achieve high accuracy of the absolute luminosity scale calibration at 8 TeV [5].

Once the calibration constants, visible cross sections σ_{vis}, for the detectors are obtained, the luminosity can be measured at any given time using the relation

$$\mathcal{L} = \frac{R}{\sigma_{\text{vis}}} \tag{1}$$

where R is the measured rate for a given luminometer.

Under usual data-taking conditions however detector acceptance effects may introduce dependencies of the calibration constants on e.g. time, the number of pile up interactions per bunch crossing μ and the filling scheme of the LHC or number of active bunches n_b.

The analysis of the first Run 2 VdM scans at 13 TeV performed in August 2015 is discussed and presented in this note. The calibration constant for the Pixel Cluster Counting method (PCC) is obtained and the associated systematic uncertainties derived.

This note is organized as follows: Section 2 decribes the PCC rate algorithm and the methods to correct for acceptance dependencies under data-taking conditions, Section 3 details the CMS August 2015 VdM scan program and analysis to determine the absolute luminosity scale calibration and associated uncertainties, Section 4 concludes on the result for the CMS Luminosity measurement for the 2015 data-taking period.

2 CMS Offline Luminosity Measurement

2.1 Pixel Cluster Counting

The PCC method has been shown to provide high precision luminosity measurements during Run 1. It is also used during Run 2 as primary offline luminometer by the CMS Collaboration. It features very low occupancy of less than a per mille under pile up environments of 25

interactions per bunch crossing.

For Run 2, the very same rate algorithm as in Run 1, namely the mean number pixel clusters per event (or bunch crossing) is used:

$$\langle N_{\text{cluster}} \rangle = \langle N_{\text{cluster/interaction}} \rangle \mu \tag{2}$$

for a mean number of interactions μ. The number of interactions based on the pp minimum bias cross σ_0 is known to be

$$\mu = \frac{\sigma_0}{f} \mathcal{L} \tag{3}$$

for instantaneous luminosity $\mathcal{L}$ and orbit frequency f. The PCC visible cross section can be defined

$$\sigma_{\text{vis}}^{\text{PCC}} \equiv \langle N_{\text{cluster/interaction}} \rangle \sigma_0 \tag{4}$$

and Eq. 2 and Eq. 3 then relates $\sigma_{\text{vis}}^{\text{PCC}}$ to the instantaneous luminosity:

$$\mathcal{L} = \frac{\langle N_{\text{cluster}} \rangle f}{\sigma_{\text{vis}}^{\text{PCC}}}. \tag{5}$$

The visible cross section is determined using the VdM scan method discussed below. For each scan point the number of clusters recorded with the zero-bias trigger is divided by the number of zero-bias events to determine the average pixel cluster rate.

All reconstructed pixel clusters are considered for counting. However, clusters reconstructed in the inner most barrel layer are affected by dynamic inefficiency of up to 1%, shown in Fig. 1a. Dynamic inefficiency is essentially buffer over-flow in pixel readout when the L1 trigger rate is very high. Generally this effect is less than 0.4% for all other pixel layers and disks as shown in Fig. 1. 0.4% is taken as a systematic uncertainty. In addition, pixel modules that are not fully operational throughout the 2015 data-taking have been omitted from the sum.

During data taking conditions, out-of-time (OOT) response affect the true mean number of pixel clusters. Fig. 2 shows single bunch instantaneous luminosities (SBIL) as measured by the PCC rate from data collected with random triggers within a typical 25ns fill. While the bunch train structure of the filling scheme is visible, a non-vanishing rate in non-active bunch slots can be observed. Two OOT response effects are distinguished and corrected for. The first effect (type 1) is due to a tail of the pixel hit signal leaking into the time integration window of the next 25ns bunch slot, which is visible in Fig. 2 in the trailing bunch slots after the trains. The second effect (type 2) is due to the exponentially decaying activation of the material surrounding the detector.

The type 2 effect was already extensively studied during the 50ns data-taking period of Run 1. Corrections for effects of type 1 are mandatory only for 25ns bunch-spacing fills. The corrections are taken to be related to the true single bunch PCC response and derived according to the correction model for type 1:

$$C_1(n+1) = \alpha R(n), \tag{6}$$

and for type 2:

$$C_2(n+j) = \beta \exp(-\lambda j) R(n), \quad j > 0, \tag{7}$$

where $R(n)$ denotes the true SBIL of bunch number n and $C_{1,2}(n)$ are the type 1,2 corrections to be applied to the SBIL of the n^{th} bunch. Based on SBIL measurements for random trigger samples recorded during 50ns bunch-spacing periods, the model parameters (α, β, λ) are estimated by minimizing the RMS of the non-active SBILs around zero. The type 2 correction model parameters are fixed for all 2015 data. The type 1 model parameter α is optimized on a fill-by-fill basis.

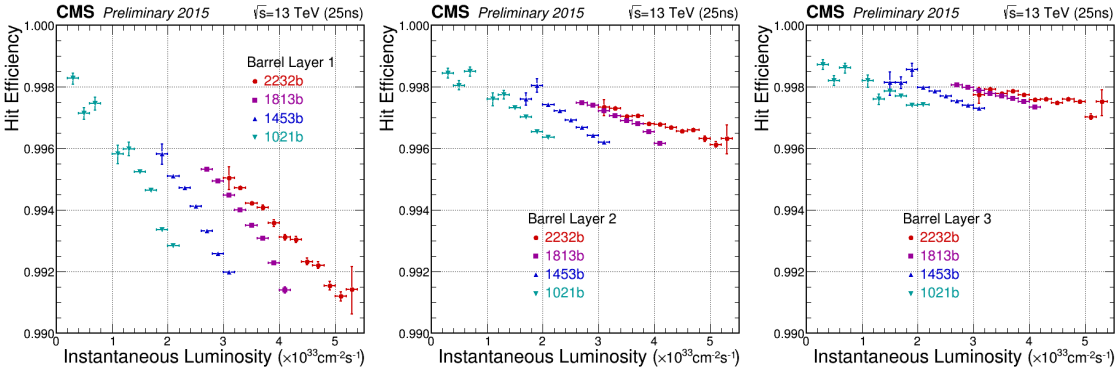

(a) Barrel Layer 1

(b) Barrel Layer 2

(c) Barrel Layer 3

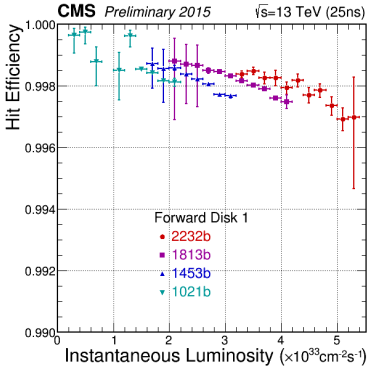

(d) Disk 1

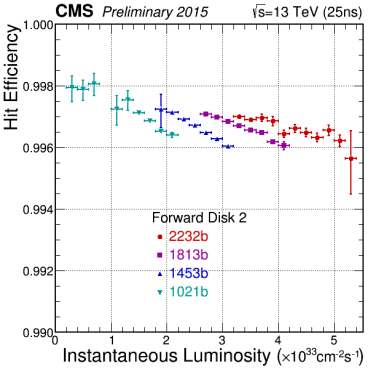

(e) Disk 2

Figure 1: Dynamic inefficiency is measured for different numbers of bunch crossings and at different total instantaneous luminosities. The efficiency is a ratio of measured pixel clusters that are associated to reconstructed tracks to predicted pixel clusters. The inefficiency is greatest at highest instantaneous luminosity and in layer 1 of the barrel reaches up to 1%. For all other regions of the pixel detector the inefficiency is less than 0.4%.

2.2 Stability and Linearity

To evaluate the long-term stability of the PCC response several studies are performed. Figure 3 shows the relative contributions of the different layers of the pixel detecors (pixel layer 1 is excluded from the PCC rate measurements) to the total PCC response over the whole 2015 data-taking period. This serves as an intrinsic cross check, and excellent stability and independence to various data-taking conditions of the different layers relative to the total response within 0.5% can be seen.

In addtion if the beam spot moves signficantly, then the acceptance of the pixel detector will change [5]. This effect would appear as a change in the visible cross section. In 2015 the beam spot was always within $\pm$2cm from the origin in the longitudinal direction. Within this range acceptance differences are negligible.

The PCC response is monitored and compared to the rate of the Muon Track Sorter of the CMS Drift Tubes trigger-system (DTLumi). The Barrel Sorter rate during the Van der Meer scan is very low, such that direct calibration is not possible. A cross calibration to PCC was performed using early 2015 data when bunches were spaced by 50 ns. PCC and DTLumi were stable in this period and the DTLumi was scaled so that the observed luminosities were equivalent on average. Figure 4 summarizes the comparison of the the two detectors over the entire 2015

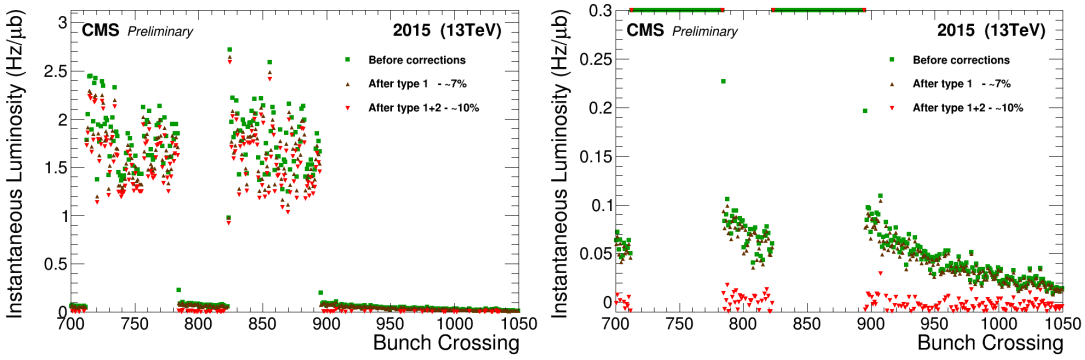

(a) PCC luminosity in run 258706

(b) Zoom on non-active BX residuals

Figure 2: Shown above are the effects of applying corrections for out-of-time pile up. First type 1 OOT is corrected followed by the type 2 correction.

data-taking period. Overall good agreement can be observed. The RMS of 1% of the ratios per LS is taken as systematic uncertainty on the stability of the PCC rate.

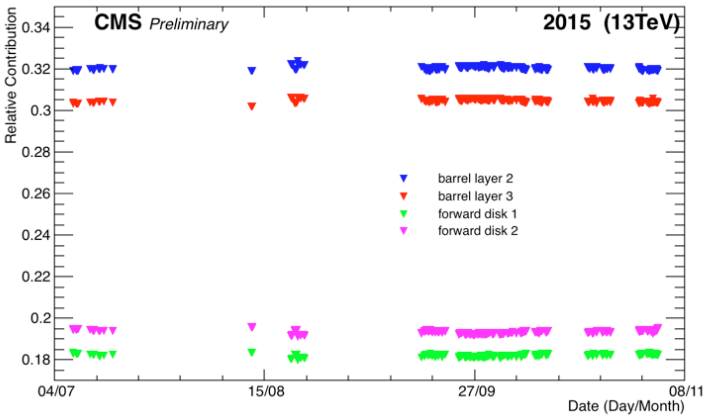

Figure 3: Relative contributions of the Pixel layers to the overall PCC rate over time.

3 2015 VdM Scan Program and Calibration Results

3.1 The VdM Scan Method

To calibrate a luminometer rate algorithm of a detector to the absolute luminosity scale, the luminosity and the luminometer rate at 13 TeV must be measured at the same time. The linear relation shown in Eq. 1 is used to determine the visible cross section (calibration constant).

The instantaneous luminosity of a colliding bunch pair separated by $(\Delta x, \Delta y)$ and assuming a vanishing z crossing-angle is defined by

$$\mathcal{L}(\Delta x, \Delta y) = N_1 N_2 f \int_{-\infty}^{\infty} \rho_1(x,y)\rho_2(x+\Delta x, y+\Delta y)\, dx\, dy \tag{8}$$

where N_1 and N_2 are the number of protons in the two colliding bunches respectively, $f = 11246$ Hz is the orbit frequency through the LHC ring and ρ_i are the proton bunch densities. While the bunch populations can be measured to good precision directly, a precise measurement of the proton bunch densities entering Eq. 8 is difficult.

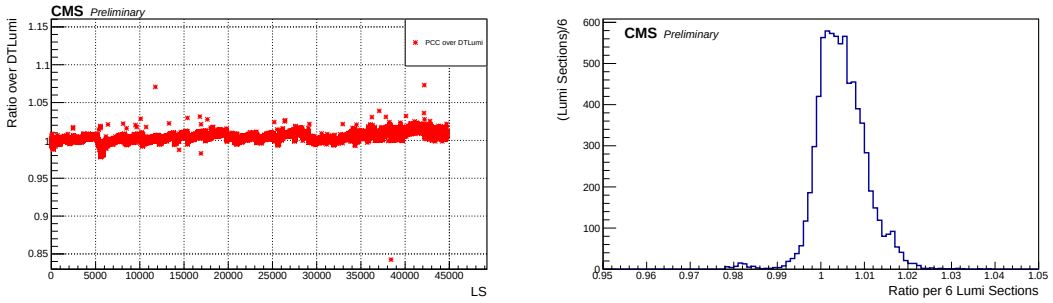

Figure 4: The ratio of CMS recorded luminosities per 6 Lumisections measured with PCC and DTLumi over the entire 2015 data-taking period as a function of time (left) and integrated over time (right).

The VdM scan method, exploited by S. Van der Meer for luminosity measurements at ISR and applied by LHC Experiments in Run 1, allows to measure and evaluate the integral over the proton bunch densities in Eq. 8.

For the VdM scan method to be applicable it is assumed that the two bunch densities factorize in x and y, i.e.

$$\int_{-\infty}^{\infty} \rho_1(x,y)\rho_2(x+\Delta x, y+\Delta y)\,dx\,dy = \int_{-\infty}^{\infty} \rho_1(x)\rho_2(x+\Delta x)\,dx \times \int_{-\infty}^{\infty} \rho_1(y)\rho_2(y+\Delta y)\,dy. \quad (9)$$

For an estimate of the possible bias introduced by this assumption, see Section 3.4.3. Both sides of Eq. 8 can then be integrated independently in Δx and Δy while the other respective separation is kept fixed, yielding

$$N_1 N_2 f \int_{-\infty}^{\infty} \rho_1(y)\rho_2(y+\Delta y_0)\,dy = \int_{-\infty}^{\infty} \mathcal{L}(\Delta x, \Delta y_0)\,d(\Delta x), \quad (10)$$

and therefore

$$\int_{-\infty}^{\infty} \rho_1(x)\rho_2(x+\Delta x_0)\,dx = \frac{\mathcal{L}(\Delta x_0, \Delta y_0)}{\int_{-\infty}^{\infty} \mathcal{L}(\Delta x, \Delta y_0)\,d(\Delta x)}. \quad (11)$$

Likewise for y. Experimentally the integration over Δx and Δy is implemented by scanning the two beams against each other and the integral on the right hand side of Eq. 10 is evaluated by measuring the luminometer rate as function of the beam-beam separation. Equation 8 then becomes Eq. 12 after replacing the beam overlap integrals in x and y according to Eq. 11 for a particular head-on working point (Δx_0,Δy_0):

$$\mathcal{L}(\Delta x_0, \Delta y_0) = N_1 N_2 f \frac{R(\Delta x_0, \Delta y_0) R(\Delta x_0, \Delta y_0)}{\int_{-\infty}^{\infty} R(\Delta x, \Delta y_0)\,d(\Delta x) \int_{-\infty}^{\infty} R(\Delta x_0, \Delta y)\,d(\Delta y)}, \quad (12)$$

where the luminosity is replaced by the measurable rate $R(\Delta x, \Delta y)$ when the two beams are separated by (Δx,Δy). It is common to re-write the integrals over the rate scan curves in terms of the convolved widths Σ_x and Σ_y of the two beams:

$$\mathcal{L}(\Delta x_0, \Delta y_0) = \frac{N_1 N_2 f}{2\pi \Sigma_x \Sigma_y}, \quad (13)$$

such that the final formular used to measure the visible cross sections is

$$\sigma_{\text{vis}} = \frac{2\pi \Sigma_x \Sigma_y R(\Delta x_0, \Delta y_0)}{N_1 N_2 f}. \quad (14)$$

All quantities on the right hand side of the above equation are measurable quantities, where in particular Σ_x and Σ_y are determined from fits of the scan curves based on luminometer rate measurements during the VdM scans. While the beam widths are the same for all luminometers, the peaks of the corresponding scan curves are luminometer dependent.

3.2 Experimental Setup

The VdM scans were performed during LHC fill 4266 at August 25th with a center-of-mass energy of 13 TeV. The LHC filling scheme was `Multi_44b_30_7_6_4bpi15nj` with 30 colliding bunch pairs at IP5 widely spread over the orbit to reduce long-range beam-beam effects and detector afterglow. LHC beam optics were adjusted to $\beta^* \approx 19$ m and transverse emittance of $\epsilon_N \approx 3.7\,\mu$m resulting in relatively wide beams of about $\sigma_b = 102\,\mu$m.

The beam intensities, about 10^{12} protons per beam, are measured with the DC Current Transformers (DCCT) [6] and the bunch currents were measured by the Fast Beam Current Transformers (FBCT) [7]. Ghost and satellite fractions are estmated by the LHC Lognitudinal Density Monitors (LDM) [8, 9]. The beam orbit was monitored using the DOROS BPMs [10] and additionally tracked using luminous region movements based on reconstructed vertices and the crossing-angle of the two beams was kept at 0 μrad.

To achieve the best statistical precision for PCC for large beam separations, CMS gated the zero-bias triggers on 5 bunch pairs (51,771,1631,2211,2674) and recorded events with a bandwidth of about 20 kHz.

The CMS VdM scan program consisted sequentially of two x-y scan pairs (X1,Y1,Y2,X2), one length scale calibration scan (LSC), one Beam Imaging scan (X3,Y3,X4,Y4), another LSC scan and one additional VdM scan pair (X5,Y5). For the 3 VdM scan pairs the two beams are put to $\pm 6\sigma_b = \pm 312\,\mu$m and scanned in 25 steps across one another in opposite directions. For the Beam Imaging scans, beam 1 (beam 2) is kept fixed at nominal position while beam 2 (beam 1) is being separated and moved in 19 steps between $\pm 4.5\sigma_b$, first in x and then in y. The time spent at each scan point is about 30 seconds. For the LSC scans the two beams are kept with fixed separation of 130 μm and simultaneously moved back and forth in the vertical and horizontal direction to derive a linear length scale correction.

The last VdM scan was about 3 hours later than the second VdM scan and is used as test for reproducibility. The Beam Imaging scans are used for specific studies on the beam shapes described in Section 3.4. Both the LSC and Beam Imaging scans are discussed in detail in [11].

3.3 Visible Cross Section Results

The size of the beam overlap is measured by fitting the scan curves, i.e. PCC and Vertex Counting rate measurements normalized by the bunch current product as a function of beam-beam separation. The scan curves are fitted with a double-gaussian model with an additional constant to fit constant background rates. For the fits to the scan curves obtained from Vertex Counting the constant term is omitted. Although fits with other functional forms were attempted the reduced χ^2 is consistently best for the double-gaussian plus constant model. The effective widths of the beam (Σ_x and Σ_y) as well as the normalized rates (R_x, R_y) are obtained per scan per bunch crossing.

For each bunch crossing the visible cross sections are then measured using Eq. 14, i.e.

$$\sigma_{\text{vis}} = 2\pi\Sigma_x\Sigma_y\langle n\rangle_0, \tag{15}$$

where

$$\langle n \rangle_0 = \frac{1}{2}(R_x + R_y), \tag{16}$$

with $R_{x,y}$ denoting the amplitudes of the fitted scan curves which are already normalized to the bunch intensities. Examples of fits to the scan curves obtained from PCC rates and Vertex Counting rates are shown in Fig. 5 and Fig. 6, respectively.

The PCC visible cross section results with statistical uncertainties of the scan curve fits are shown in Fig. 8. The values for the visible cross sections are consistent within statistical uncertainties, both, on average per scan and per bunch crossing. A direct comparison of the beam widths obtained from PCC and vertex counting scan curves is shown in Fig. 7. The compatibilty is very good with an average difference of 0.04% in the measured beam widths. Also shown are the measured Σ_x and Σ_y for all five bunch crossings and four scan pairs separately. Σ_y decreases by about 3% during the scan campaign and the overall beam width decreases for bunch crossings towards the end of the orbit. These trends however do not affect the visble cross section measurements.

The overall cross section is determined from the weighted mean of all five cross sections per bunch crossing from the four scans to be $\sigma_{\text{vis}}^{\text{PCC}} = 8.992 \pm 0.007$ barn.

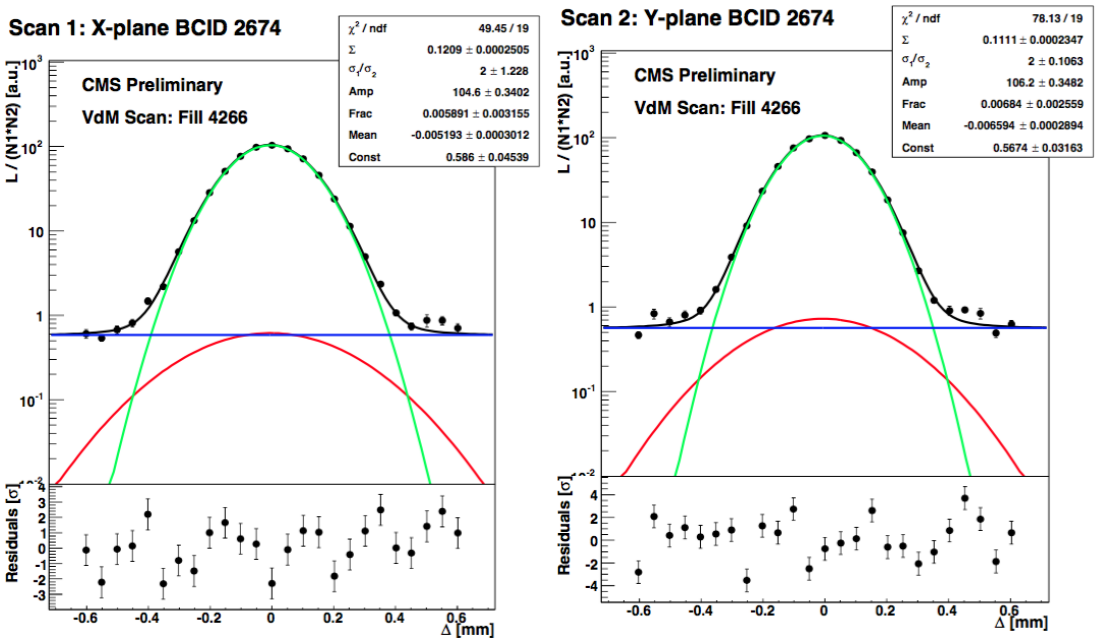

Figure 5: Shown are the fitted scan curves recorded by PCC during X1 (left) and Y1 (right) for bunch crossing 2674.

3.4 Corrections and Systematic Uncertainties

3.4.1 Length Scale Calibration

To enhance the precision on the beam separation derived from the LHC orbit knobs, the beam-spot movements reconstructed by the CMS tracking system are measured and corrections to the beam separation are derived. While the LHC orbit knobs may suffer from hysteresis effects, the position of the beam-spot can be reconstructed with sub-micron accuracy. The data recorded during the two vertical and horizontal LSC scans, explained in Section 3.2, are used. The procedure to derive the length scale calibration constants follows the method already used in previous analyses [11, 12]. The beam-spot movement as a function of the nominal offset

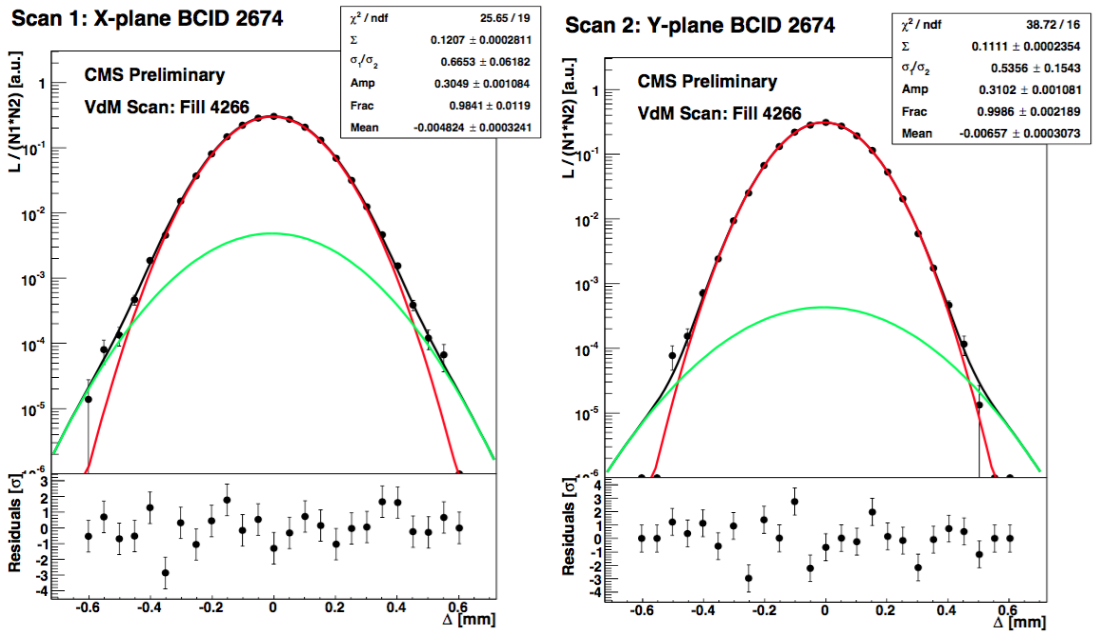

Figure 6: Shown are the fitted scan curves of the vertex rates during X1 (left) and Y1 (right) for bunch crossing 2674.

of the beam centroid is fitted with a straight line and a calibration constant extracted. This is depicted in Fig. 9 for LSC scan in the horizontal and vertical direction. In both transverse coordinates, the fits produce slopes of on average 0.983 in the horizontal scans and 0.985 in the vertical scans. These corrections are applied directly to beam-beam separations in the scan curves and effectively reduce the measured beam width by 1.7% horizontally and 1.5% vertically. The measured visible cross section is therefore reduced by 3.2% with this correction. A 1.5% uncertainty is assigned until the calibration is validated by future scans in 2016.

3.4.2 Orbit Drift

Significant orbit drift of the beams away from their fixed orbit position is observed during the first Beam Imaging scan pair (X3,Y3). Figure 10 shows the difference of the beam orbits from before and after each scan. The size of the effective area obtained in this scan is systematically smaller compared to the other four scans by about 2%. The orbit drift as estimated by the DOROS BPM is studied in simulation and found to cause a decreased effective area of that size. The first Beam Imaging scan is therefore not considered in the overall PCC visible cross section estimates. Both the vertical and horizontal beam orbit drift during the other four scans is very small, below 3 μm, which can have an impact of at most 0.4%. This is taken as an uncertainty and no further corrections are applied.

3.4.3 XY-Correlations

The assumption that the proton bunch densities are factorizable in x and y made for the VdM scan method, c.f. Eq. 9 is not valid in general and may result in an over estimation of the beam overlap integral [4]. To estimate the size of this potential bias in the 2015 VdM scan, the 2 dimensional distributions of reconstructed vertices in the transverse plane of the CMS Detector recorded during the Beam Imaging scans are exploited [13]. The pull distribution of a single-gaussian proton bunch density model to the vertex distribution accumulated during scan Y3 is shown in Fig. 11 where signs for non-factorizable beam shapes can be observed.

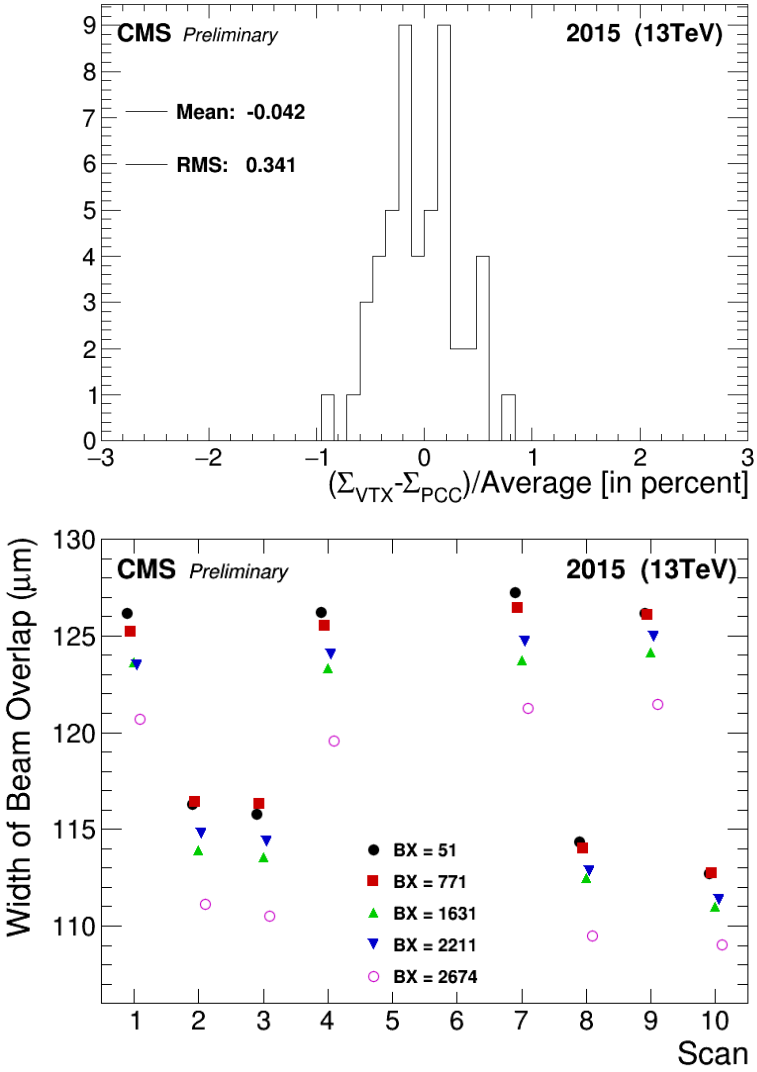

Figure 7: Comparison of horizontal and vertical beam widths obtained from PCC and vertex counting (left) and beam widths as a function of scan and BCID (right).

The vertex distributions are then fitted using a double-gaussian bunch density model for each bunch crossing separately allowing for correlation parameters to vary. An example of the pull distribution is shown in Fig 11. A simulated VdM scan with the extracted bunch densities is then performed to find good agreement with the beam overlap integrals obtained from the measured scan curves in Section 3.3. An overall correction of 1.1% to the visible cross section is derived, based on the per-BCID comparison of the full beam-overlap integral in the two-dimensional plane to the effective areas estimated using the VdM scan method. The systematic uncertainty associated to this procedure is estimated to be 1.5%.

3.4.4 Beam-Beam Effects

The strengths of the mutual electromagnetic forces of the two colliding positively charged bunches change as a function of separation and, if uncorrected, can bias the results obtained from the VdM scans. The two beams repel each other (beam-beam deflection) changing the actual beam separation during the scans. Figure 12 shows the change in separation as a function of nominal separation, calculated using the procedure from [14]. A correction to the beam-beam

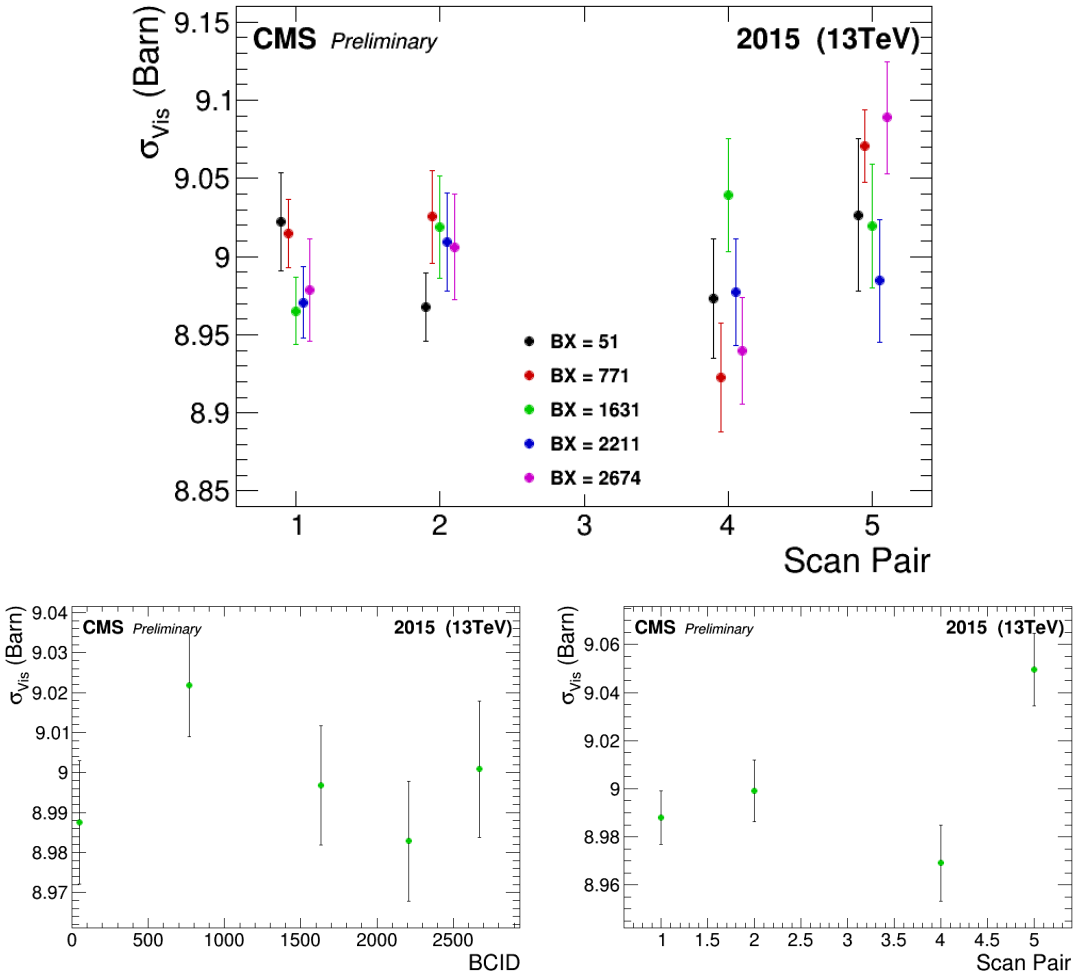

Figure 8: The upper plot shows resulting cross sections with statistical error for all bunch crossings measured in all scans. The lower left is the weighted average of PCC visible cross sections per bunch crossing. The lower right plot depicts the weighted average of visible cross sections per scan.

separation in the scan curves is applied per scan and bunch crossing accordingly, resulting in an overall correction of about 1.8% on the visible cross section. The uncertainty on this calculation is dominated by the uncertainty on β^*, which we assume is $\sim$ 20%. The uncertainty of this beam-beam correction is 0.4%. Apart from the beam-beam deflection, the electromagnetic forces give rise to de-focussing effects (dynamic-β) of the proton bunch densities varying as function of distance. This effect is however expected to be small, and an uncertainty of 0.5% is assigned to cover the possible impact on the visible cross section measurement. The overall uncertainty due to beam-beam effects is 0.6%.

3.4.5 Bunch Current Normalization

The bunch current normalization is measured by the FBCT with per-bunch slot granularity. The FBCT is cross calibrated to the total intensity of the beam current product measured by the DCCT. Ghost contributions enter the total beam intensity measurement and satellites contribute to FBCT bunch current measurement without contributing to the instantaneous luminosity. These contributions are however estimated to be very small 0.11% for beam 1 and 0.07% for beam 2, therefore no correction is applied but instead an uncertainty of 0.2% is assigned to

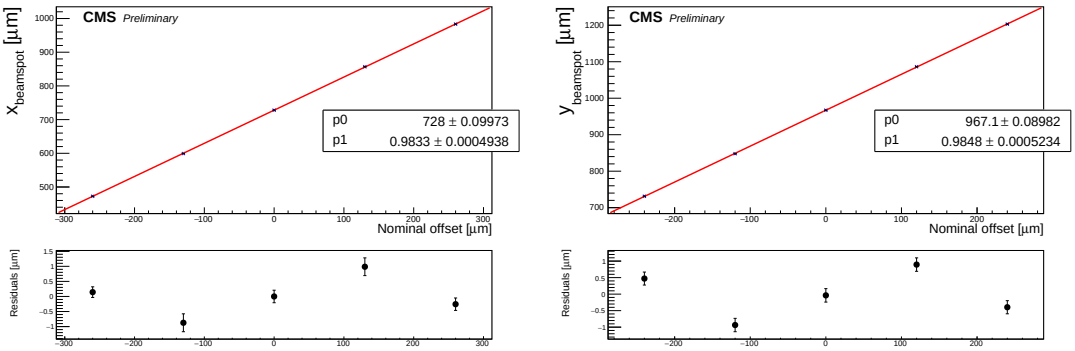

Figure 9: Examples of the measured beam-spot position as a function of the beam centroid offset are shown for a horizontal (left) and vertical (right) LSC scan. The points are fitted with a straight line to derive the LSC constant.

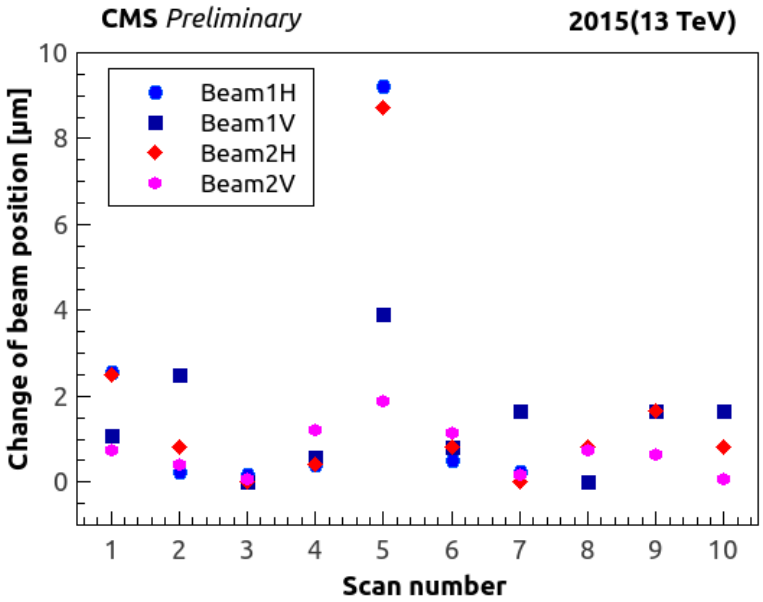

Figure 10: The difference of the two vertical and horizontal beam orbits from before and after each scan as measured by the DOROS BPM in μm is shown.

the bunch population. DCCT measures the current of the beam product with a precision of 0.3%, which is taken as an additional systematic uncertainty.

4 Conclusions

The analysis of the VdM scans performed by the CMS Collaboration in August 2015 for the calibration of the Pixel Cluster Counting rate to the absolute luminosity scale for p-p collisions at $\sqrt{s} = 13$ TeV and a magnetic field strength of 3.8 T in the detector is presented. Acceptance effects affecting the Pixel Cluster rate over time are identified and corrections derived.

Table 1 summarizes the corrections and systematic uncertainties discussed in Sections 3.4 and 2. The various sources are grouped into uncertainties entering the normalization, i.e. luminosity scale calibration during the VdM scan procedure, and uncertainties entering the stability of the PCC rate over time.

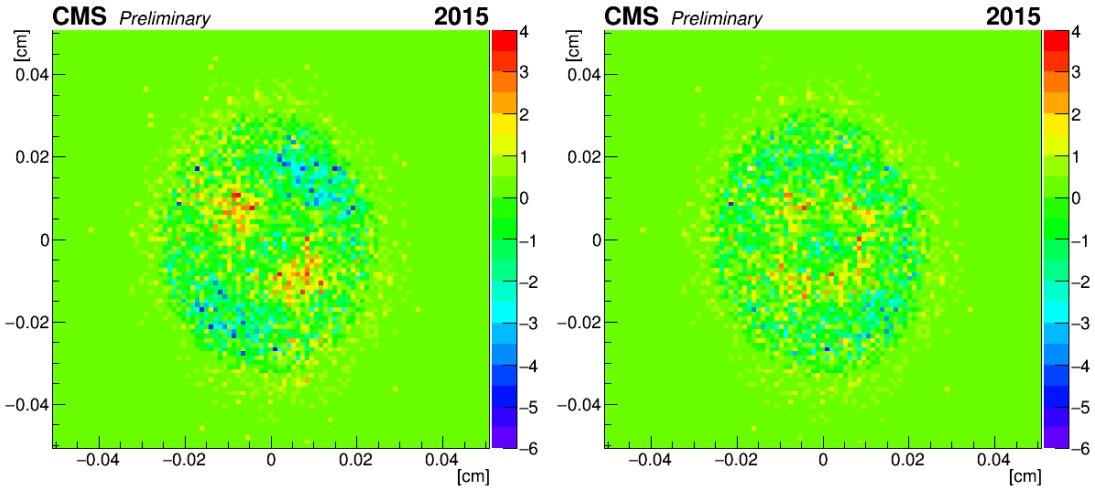

Figure 11: Example of a pull distribution of the fitted model of single gaussian (left) and double gaussian (right) type to the vertex distribution accumulated during scan Y3 of bunch crossing 1631.

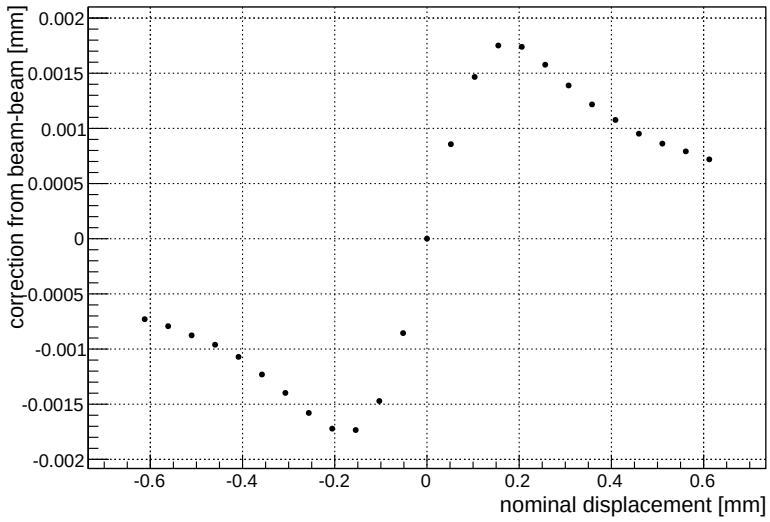

Figure 12: Shown is an example of beam-beam deflection estimates as a function of beam-beam separation.

The dominating uncertainties contributing to the luminosity scale calibration are associated to the length scale calibration of the beam-beam separations and non-factorizability of the colliding proton bunch densities. All normalization uncertainties are treated uncorrelated and total 2.3% on the luminosity scale calbration.

The integration uncertainty incorporates the uncertainties associated to the extrapolation of the PCC visible cross section to PCC rate measurements under usual data-taking conditions as discussed in Section 2. In addition, an uncertainty of 0.5% associated to the deadtime estimate of the CMS DAQ system is included affecting the recorded integrated luminosity.

The uncertainties on the integration and normalization are treated as uncorrelated. In summary, the total uncertainty on the CMS luminosity measurement in 2015 is estimated to be 2.7% for CMS data recorded with 3.8 T magnetic field strength and proton-proton collisions at

$\sqrt{s} = 13$ TeV.

Table 1: Summary of the systematic uncertainties entering the CMS luminosity measurement for 13 TeV proton-proton collisions. When applicable, the percentage correction is shown.

	Systematic	correction (%)	uncertainty (%)
Integration	Stability	-	1
	type 1	$7-9$	0.6
	type 2	$0-4$	0.7
	CMS deadtime	-	0.5
	Dynamic Inefficiency	-	0.4
Normalization	XY-Correlations	1.1	1.5
	Beam current calibration	-	0.3
	Ghosts and satellites	-	0.2
	Length scale	-3.2	1.5
	Orbit Drift	-	0.4
	Beam-beam deflection	1.8	0.4
	Dynamic-β	-	0.5
	Total		2.7

References

[1] S. van der Meer, "Calibration of the effective beam height in the ISR", Technical Report CERN-ISR-PO-68-31. ISR-PO-68-31, CERN, Geneva, 1968.

[2] ALICE Collaboration, "Measurement of visible cross sections in proton-lead collisions at $\sqrt{s_{\rm NN}}$ = 5.02 TeV in van der Meer scans with the ALICE detector", *JINST* **9** (2014), no. 11, P11003, doi:10.1088/1748-0221/9/11/P11003, arXiv:1405.1849.

[3] ATLAS Collaboration, "Improved luminosity determination in pp collisions at sqrt(s) = 7 TeV using the ATLAS detector at the LHC", *Eur. Phys. J.* **C73** (2013), no. 8, 2518, doi:10.1140/epjc/s10052-013-2518-3, arXiv:1302.4393.

[4] LHCb Collaboration, "Precision luminosity measurements at LHCb", *JINST* **9** (2014), no. 12, P12005, doi:10.1088/1748-0221/9/12/P12005, arXiv:1410.0149.

[5] "CMS Luminosity Based on Pixel Cluster Counting - Summer 2013 Update", Technical Report CMS-PAS-LUM-13-001, CERN, Geneva, 2013.

[6] P. Odier, M. Ludwig, and S. Thoulet, "The DCCT for the LHC Beam Intensity Measurement", Technical Report CERN-BE-2009-019, CERN, Geneva, May, 2009.

[7] D. Belohrad et al., "The LHC Fast BCT system: A comparison of Design Parameters with Initial Performance", Technical Report CERN-BE-2010-010, CERN, Geneva, May, 2010.

[8] A. Jeff et al., "Longitudinal density monitor for the LHC", *Phys. Rev. ST Accel. Beams* **15** (Mar, 2012) 032803, doi:10.1103/PhysRevSTAB.15.032803.

[9] A. Jeff, C. Welsch, and A. Boccardi, "A Longitudinal Density Monitor for the LHC". PhD thesis, Liverpool U., Dec, 2012. Presented 11 Dec 2012.

[10] M. Gasior, J. Olexa, and R. Steinhagen, "BPM Electronics based on Compensated Diode Detectors Results from development Systems", *Conf. Proc.* **C1204151** (Apr, 2012) MOPG010. 3 p.

[11] M. Zanetti, "Beams Scan based Absolute Normalization of the CMS Luminosity Measurement. CMS 2010 luminosity determination", Technical Report CERN-Proceedings-2011-001, CERN, Geneva, Jan, 2011.

[12] CMS Collaboration Collaboration, "CMS Luminosity Based on Pixel Cluster Counting - Summer 2012 Update", Technical Report CMS-PAS-LUM-12-001, CERN, Geneva, 2012.

[13] J. Salfeld-Nebgen, M. Klute, and C. A. Medlock, "Beam Imaging and Luminosity Calibration", Technical Report CERN-OPEN-2016-003, CERN, Geneva, Mar, 2016.

[14] W. Kozanecki, T. Pieloni, and J. Wenninger, "Observation of Beam-beam Deflections with LHC Orbit Data", Technical Report CERN-ACC-NOTE-2013-0006, CERN, Geneva, Aug, 2013.